OPTIMIZED PULSING OF HIGH-INTENSITY FOCUSED ULTRASOUND FOR ENHANCED THERAPEUTIC WINDOW

A THESIS
SUBMITTED TO THE FACULTY OF THE GRADUATE SCHOOL
OF THE UNIVERSITY OF MINNESOTA BY

Muhammad K. Al-Qaisi

IN PARTIAL FULFILLMENT OF THE REQUIREMENTS
FOR THE DEGREE OF
MASTER OF SCIENCE IN BIOMEDICAL ENGINEERING

Advisor: Emad Ebbini

March 2010

Acknowledgements

I would like to thank everybody who helped having this work done. First, I thank my adviser, Prof. Emad Ebbini, for his valuable mentorship. The diversity of his suggestions has opened many purviews for investigations. I also want to thank my Ph.D. mentor, Prof. Taner Akkin, for his flexibility with me going through this work. A lot of appreciation is extended to Professor James Leger for his openness and availability for general discussions. I also prize the willingness of Prof. John Bischof to be on this committee and provide precious feedback.

Thanks to every lab member: Brett Otteson, Hanwoo Lee, Kalyani Mallela, Mohamed Al-Mekkawy, Yayun Wan, John Ballard, Ajay Shrestha and Vijay Aditya; theirs company was always joyful. Special thanks to Dalong Liu whom I used some of his instrumentation, and Andrew Casper for his precious assistance in getting started with COMSOL. I strongly appreciate the feedback from Hui Wang, my Ph.D. labmate, in preparing the presentation.

I must thank my parents and siblings for their constant support and availability to help; the good environment they created is cherished. Very sincere thanks to my wife whose support and endorsement where the main stimulus to have this work finished. Thanks Mysoon for being always the best despite the weekends I have spent away wrapping this manuscript up. Finally, I thank the Jordan University of Science and Technology for the scholarship that has, in most part, funded me during this work.

Abstract

High intensity focused ultrasound (HIFU) provides a unique modality to perform non-invasive surgeries. The thermal ablation technique relies on focusing the non-ionizing acoustic wave within soft tissues to produce a small lesion. HIFU operations are typically attempted by continuous-wave (CW) applications of the beam intervened by wait periods to allow surrounding tissue to cool down. Large contiguous lesions are produced by raster-scanning the beam over the volume of the tumor; a procedure that requires up to three hours for a 2-cm diameter tumor. This is one of the main limitations of HIFU thermal therapy. As part of the ongoing research to accelerate the procedure, we investigate the role of pulsed-HIFU (pHIFU) parameters in the enhancement of the *therapeutic gain* within the HIFU focus. A *therapeutic gain* is observed when high duty cycle pHIFU is pulsed at the mechanical resonance of the medium. Up to 50% increase in temperature was measured in lab-prepared tissue mimicking phantoms. The *therapeutic gain* achieved by pHIFU over cwHIFU is attractive as no modifications on the currently used applicators are required.

Table of contents

List of Figures

Chapter 1: Introduction

The application of ultrasound technology in health care is evolving. Common applications are the well-known sonography, intravascular ultrasound imaging [Tobis 1991], ultrasound microscopy [Foster 1993], drug delivery [Tachiabana 2001], and various therapeutic applications. The non-ionizing propagation of the wave in soft tissues suggests its safety for use in living tissues. In high-intensity focused ultrasound (HIFU), however, high levels of acoustic energy can be deposited at focus resulting in ablation or thermal necrosis in tissues receiving sufficient thermal dose [Saparato 1984]. The feasibility of HIFU application for non-invasive surgeries has received significant attention since the early 1990s [Kennedy 2003]. Previous studies have suggested the technique for beating heart ablation to treat atrial fibrillation [Schmidt 2006, Ninet 2005], and tissue ablation procedures [Wu 2003, Arifiev 1998]. In a breast cancer study [Wu 2003], pathologic findings revealed that HIFU-treated tumor cells underwent complete coagulative necrosis, and tumor vascular vessels were severely damaged. Immunohistochemical staining has indicated that the treated tumor cells lost their ability of proliferation, invasion, and metastasis. Other applications extend to gene therapy [Frenkel 2006, Dittmer 2005], and drug delivery [Dromi 2007].

Absorption of acoustic energy results in heating of the medium with the temperature evolution governed by the transient bioheat equation (tBHTE) [Pennes 1948], which is a modified version of the parabolic heat equation. The acoustic source in the tBHTE is αI_{SPTA}, where α is the absorption coefficient [Goss 1979] and I_{SPTA} is the spatial-peak temporal-average intensity of the sound beam (in W/cm^2). At intensity levels on the order of (10^2 W/cm^2) and exposure durations in the range of 30 – 60 minutes, localized hyperthermia can be produced using focused beams in the low MHz frequency range. At intensity levels on the order of (10^3 W/cm^2) and exposure durations

in the range of 2 – 10 seconds, localized tissue necrosis can be produced using focused beams in the 1 – 10 MHz range. This mode of tissue ablation/coagulation has received increased attention during the last two decades and research in this area has resulted in a number of clinical systems, e.g. for the treatment of prostate cancer and uterine fibroids.

Current clinical systems employing HIFU rely on the thermal tissue response to continuous-wave (CW) application of the beam to produce a small lesion in response to 5 – 10 second exposure (commonly referred to as shot) followed by 20 – 50 second wait to allow the intervening/surrounding tissues to cool down. A volumetric contiguous lesion covering the tumor can be produced by raster scanning single shots to produce a closely-packed array of small lesions. Given the volume of the single-shot lesions is in the range of 15 – 30 mm^3, a 2-cm diameter tumor may require hundreds of shots requiring treatment times in the range of 2 – 3 hours. This is one of the main limitations of HIFU-based thermal therapy. This limitation has triggered a number of research efforts to accelerate the single-shot lesion formation by minimizing the wait time between shots. One way is to increase the power output of the HIFU applicator. This approach is limited by the characteristics of piezoelectric crystal, and more importantly, by prefocal heating due to linear (heat conduction) and nonlinear (intensity saturation[1]) phenomenon.

Another approach is to optimize the efficiency by maximizing acoustic wave absorption as a thermal form of energy. In biological tissues, acoustic energy is absorbed into thermal and mechanical forms of energy. Part of the mechanical energy is expressed as shear waves (described in the Chapter 2). Due to the incompressible nature of soft tissues, shear waves experience high attenuation and local absorption, in the form of heat. If continuous creation and

[1] Intensity saturation refers to the generation and absorption of higher order harmonics in the tissues proximal to the HIFU transducer, i.e. prior to reaching the geometric focus.

absorption of shear waves was maintained over the treatment window, the shear-wave mechanical energy will be transformed into thermal. In other words, the viscoelastic properties of soft tissues might be exploited to enhance heat generation.

This resonance condition can be met by pulsed-HIFU (pHIFU) operation. If appropriate pulsing parameters are applied, the resonance can be maintained. We investigate the role of pHIFU in the enhancement of the *therapeutic gain* within the HIFU focus with respect to the intervening/surrounding tissue. In particular, we investigate the role of pulse-repetition frequency (PRF) and duty cycle (DC) of the pHIFU in enhancing the temperature rise at the focus compared to the standard cwHIFU shot of the same duration and energy.

Chapter 2: Background

Acoustic waves propagate in soft tissues at speeds between 1510 and 1645 m/s [Mast 2000], close to its propagation speed in water. This is equivalent to wavelengths on the order of hundreds of micrometers for HIFU procedures; which is relatively large when compared to many tissues heterogeneity. Hence, many tissues like liver and muscles behave like homogenous propagation media for the acoustic propagation. Nevertheless, and owing to different factors, the study of acoustic wave interaction with tissues is complicated. Factors believed to influence the outcome of this study are presented in this chapter.

First, attenuation of the acoustic wave is due to absorption and scattering. The contribution of scattering coefficient to total attenuation, however, varies between 0.1% in blood and 20% in human liver [Nassiri 1986] for frequencies close to those used in HIFU. Therefore the influence of the scattering coefficient will be neglected, and the equations used here assume that the attenuation and the absorption coefficient are equal. The absorption coefficient α is a function of frequency and is approximated as $\alpha \approx \alpha_0 f^n$, where f is the acoustic frequency in MHz, α_0 is the absorption coefficient at around 1 MHz, and n is a constant lies between 1 and 2 depending on tissue [Cobbold 2006, P. 74]. This means that higher frequency components are absorbed at higher rates, which results in higher temperature elevation per unit intensity.

Second, acoustic waves in water and soft tissues are compression waves. This means that the propagation of the wave applies a force, and hence a pressure, on the particles of the medium [Cobbold 2006, P. 7]. This radiation force generates shear waves near HIFU focus [Cobbold 2006, P. 560]. Shear waves are low-frequency lateral vibrations. Due to incompressibility of biological tissues, shear waves experience high attenuation coefficient and, therefore, vanish within a few wavelengths distance [Sarvazyan 1998]. The mechanical energy of the shear wave is

absorbed as heat. In this work, we employ the absorption of shear waves as heat to achieve HIFU *therapeutic gain*. Shear wave generation and properties are described in Section 2.3.

Nonlinear wave-tissue interaction is another important factor in heat generation. As the acoustic wave propagates in the medium, harmonic generation (nonlinearity) occur even at low intensities. As described above, higher harmonics experience a higher attenuation coefficient. Therefore, nonlinearity -briefly described in Section 2.4- can potentially play an important role in the outcome of this study.

2.1 The Bioheat equation

In HIFU procedures, heat is mainly generated by direct absorption of acoustic waves as thermal energy. Heat absorption and diffusion, and transient temperature changes are all described in the transient Bioheat equation [Pennes 1948]:

$$\rho_0 C_p \frac{\delta T}{\delta t} + \nabla(-k\nabla T) = Q \tag{1}$$

The heat source Q is calculated as $2\alpha I$ [Cobbold 2008], where α is the absorption coefficient, and I is the acoustic intensity. The first term from the left describes transient temperature changes where C_p is the heat capacity of the medium, ρ_0 is the density of the medium, T is the temperature, and t is the time. In the second term from the left, k is the thermal conductivity, and $-k\nabla T$ is the heat flux vector.

To study the temperature frequency response to pHIFU at a single point in space, the acoustic intensity is written as a function of time $I(t)$. Therefore, the heat source Q is also a function of time $Q(t)$, and the Bioheat equation can be rewritten as:

$$\rho_0 C_p \frac{\delta T(t)}{\delta t} - k\nabla^2 T(t) = Q(t) \tag{2}$$

when *k* is assumed constant. In the frequency domain, Equation (2) takes the form:

$$T(s) = \frac{Q(s) + \rho_0 C_p T(t_0)}{\rho_0 C_p s} \tag{3}$$

where $T(t_0)$ is the initial temperature before pHIFU application. The same result was shown earlier in [Ebbini 1990].

When $s = i2\pi f$, where f is the pulsing frequency, it is obvious from Equation (3) that the change in temperature due to the heat source Q decays with frequency in $1/f$ form. In other words, temperature response is an integration of the acoustic stimulus, and it only responds to the temporal average of the stimulus. At the frequency range used in the experiments described in the following chapters (200 – 800 Hz), response to modulation is at least 200 times lower than the response to mean stimulus. Hence, the heat source term is usually calculated based on the spatial-peak temporal-average intensity (I_{SPTA}) as $2\alpha I_{SPTA}$, and the direct heat source (Q) contribution is independent from PRF.

2.2 Acoustic radiation pressure and radiation force

Propagation of acoustic waves in an attenuating medium generates pressure waves according to Tait equation [Lee 1993]:

$$p = Q_0[(\rho/\rho_0)^{\Gamma} - 1] \tag{4}$$

where p is the acoustic pressure, ρ_0 is the ambient density of the medium, $\rho = \rho_0 + \rho_{ac}$, and ρ_{ac} is the acoustic density. Γ is a constant and Q_0 is equal to $\rho_0 c_0^2/\Gamma$, where c_0 is the ambient speed of sound. For water $\Gamma = 7$ and $Q_0 = 3000$ bars. Taylor expansion of the Tait equation yields:

$$p = A\left(\frac{\rho_{ac}}{\rho_0}\right) + \frac{B}{2!}\left(\frac{\rho_{ac}}{\rho_0}\right)^2 + \frac{C}{3!}\left(\frac{\rho_{ac}}{\rho_0}\right)^3 \ldots \quad (5)$$

where $A = \rho_0 c_0^2$, $B = (\Gamma - 1)\rho_0 c_0^2$, and $C = (\Gamma - 1)(\Gamma - 2)\rho_0 c_0^2$. It is clear that $B/A = (\Gamma - 1)$ and $C/A = (\Gamma - 1)(\Gamma - 2)$.The first order measure of nonlinearity, *B*/*A*, is a common measure of the severity of nonlinear generation. The ratio *B*/*A* is known as the nonlinear parameter.

A preserved linear relationship between pressure and density guarantees an oscillatory component varying with the acting acoustic wave, and averages to zero. In case of nonlinear relation between pressure and density in the medium, a steady state component known as the radiation pressure is observed [Cobbold 2007, P. 45]. Since pressure is the amount of force acting on a unit area, the terms (radiation pressure and radiation force) maybe interchangeably used hereafter. In case of HIFU, shear waves are generated due to the acoustic radiation force.

2.3 Shear waves

Lateral shear oscillations can be generated by the radiation force produced by HIFU transducers. It was shown that shear waves, under some conditions, follow a second order transfer function and exhibit low frequency response [Sarvazyan 1998]. Liu and Ebbini have demonstrated experimentally that shear-wave has a low frequency resonance (roughly between 100 and 1000 Hz) that depends on the stiffness of the tissue, and its boundary conditions [Liu 2008]. Figure 1 (courtesy Dalong Liu) shows the frequency response of tissue-mimicking phantoms exhibiting the different levels of stiffness and different thicknesses. It is clear from the figure that resonance exists, and it varies with the properties of the tissue and its boundaries. In addition, the results show that the resonance frequency is measurable.

Homogeneous unbounded soft tissues exhibit viscoelastic properties with resonance frequencies in the 10s of Hz. In the presence of rigid boundaries, however, the resonance frequencies can reach 100s of Hz as suggested by Figure 1. In general, the structure and the heterogeneity of the target tissues for HIFU treatment may have unknown resonance frequencies, but these can be measured using the methods described in [Liu 2008]. Once the resonance frequency of the target tissue is known, HIFU beam can be easily pulsed with matching modulation frequency to maximize the shear wave generation near the HIFU focal spot. Given the high attenuation of the shear waves(up to 12 dB/cm for rubber phantoms at 5 Mhz [Sarvazyan 1998]), we hypothesize that the generation of shear waves will result in increased power deposition (increased *therapeutic gain*) in the vicinity of the focal spot. This may help in increasing both the localization and the speed of the lesion formation processes.

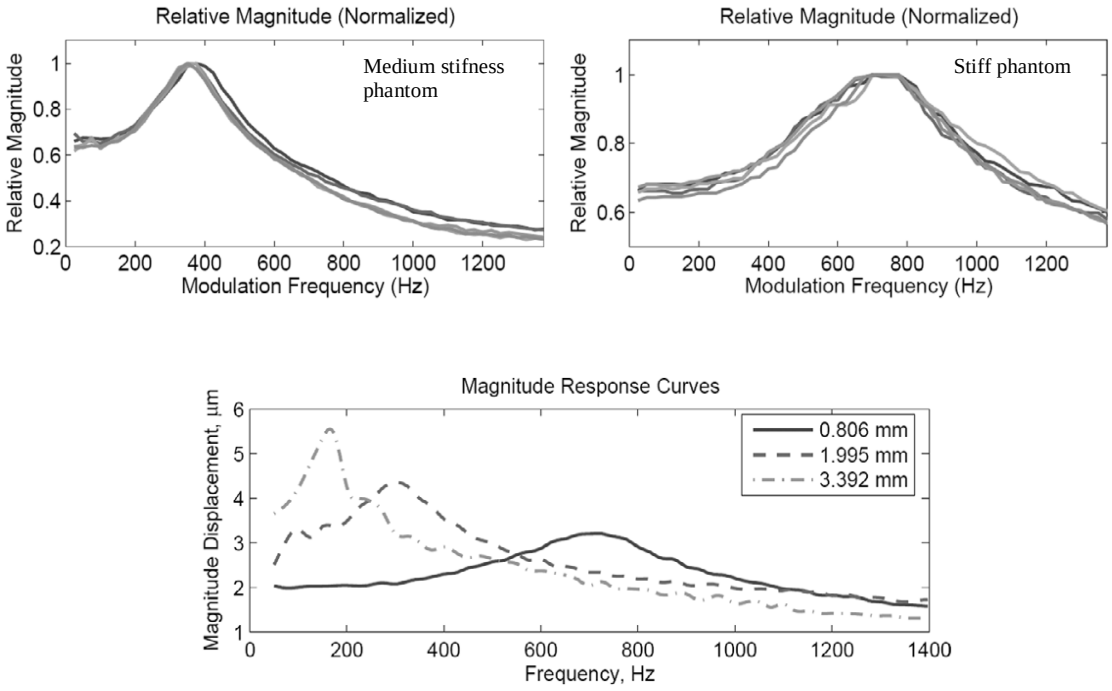

Figure 1 Shear-waves frequency response in phantoms having different moduli of elasticity *E* (top left: *E* = 0.5 kPa, top right *E* = 1.6 kPa), and different thicknesses (bottom). **(**Courtesy: Dalong Liu)

Because of the high shear wave attenuation coefficient, they are fully-attenuated after propagating a few wavelengths. Since they diminish within a small area, shear-waves localization was suggested for high-resolution imaging [Sarvazyan 1998]. This means that the besought therapeutic gain will also exhibit high level of localization. The spatiotemporal course and localization advantage of shear waves are shown in Figure 2 (source Sarvazyan 1998). Note the short attenuation length in the lateral dimension.

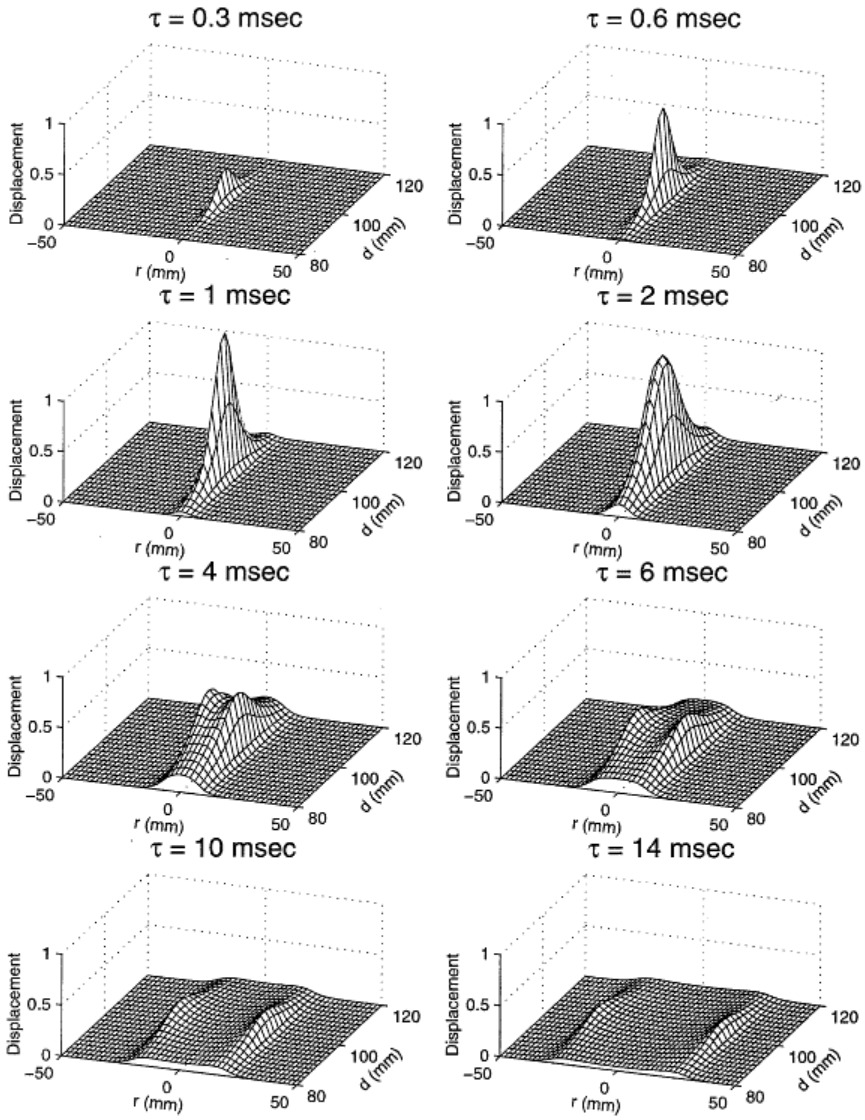

Figure 2 Shear wave dissipation calculated as a function of space and time (Source: Sarvazyan et al., 1998)

2.4 Nonlinearity

Nonlinear wave-tissue interaction was not originally a part of this study. Nevertheless, and due to the operating conditions of the experiments, harmonics generation and absorption had an influence on the results. The nonlinear wave-tissue interaction has a strong influence the conversion of the acoustic energy into thermal [Muir, 1980]. An experimental model has suggested the nonlinear interaction is the reason of increased heat generation in HIFU [Swindell, 1985]. Another *in vivo* study has confirmed the potential benefit of nonlinear acoustic absorption in clinical operations [Hynynen, 1985].

Nonlinear interaction may, however, result in prefocal heating and hence lower temperature increase at focus. The second harmonic, for example, will be absorbed faster and will not travel as far as the fundamental. This means enhanced heating can be generated if harmonics were created at focus, but can also result in undesired prefocal heating if harmonics were absorbed earlier [Swindell 1985]. Nonlinear effects are not limited to absorption coefficient and proximity to focus. Due to diffraction, the beam waist at HIFU focus is tighter at higher frequency [Muir 1980, Swindell 1985, Hynynen 1985]; suggesting a smaller focal volume for higher harmonics.

Chapter 3: Materials and methods

3.1 HIFU transducer

A highly-focused lead zirconate titanate (PZT) HIFU transducer with a spherical section of 12 mm diameter was used as a HIFU source [Liu 2008]. The dual-element transducer has an imaging element which was not used in any of the experiments described here. The HIFU transducer focus has a cigar shape with around 1 mm full-width half-max (FWHM) axial length, and 200 µm lateral FWHM diameter. Due to the complex impedance mismatch between the power source and the transducer, an RC matching circuit was designed to nullify the imaginary voltage component at the operation frequency. Therefore, the power reflected from the transducer was minimized. A set of experiments were launched to test the electrically-matched transducer.

The conductance of the electrically-matched transducer was measured using Agilent's 4395A network analyzer. Figure 3 shows the measured conductance of the transducer in both air and water. The crystal resonance is shown at 5 MHz. The quality factor ($Q = f_{\text{res}} / \Delta f_{\text{FWHM}}$, where f_{res} is the resonance frequency, and Δf_{FWHM} is the full-width half-maximum bandwidth) is lower when the transducer is immersed in water. This is because of the increased acoustic energy dissipation in water. A better acoustic impedance matching, if added, will improve the efficiency of energy transfer at the interface and further reduce the Q-factor.

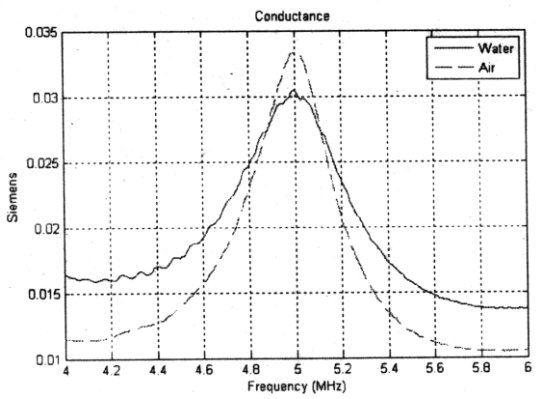

Figure 3 Conductance of the electrically-matched transducer measured both in air and water

To measure the ultrasound power of the transducer, its efficiency, and its temporal stability, the stimulation was generated using HP 33120A function generator. A radio-frequency (RF) power amplifier (A150) feeds the transducer through a directional power meter (Bird 4410) that measures both forward and reflected electrical power. Ultrasound power was measured using a calibrated ultrasound power meter (Ohmic UPM-DT-100AV). The setup is shown in Figure 4. The frequency response of the transducer was confirmed by measuring the acoustic power while changing the electrical frequency applied to the transducer. The output is shown in Figure 5.

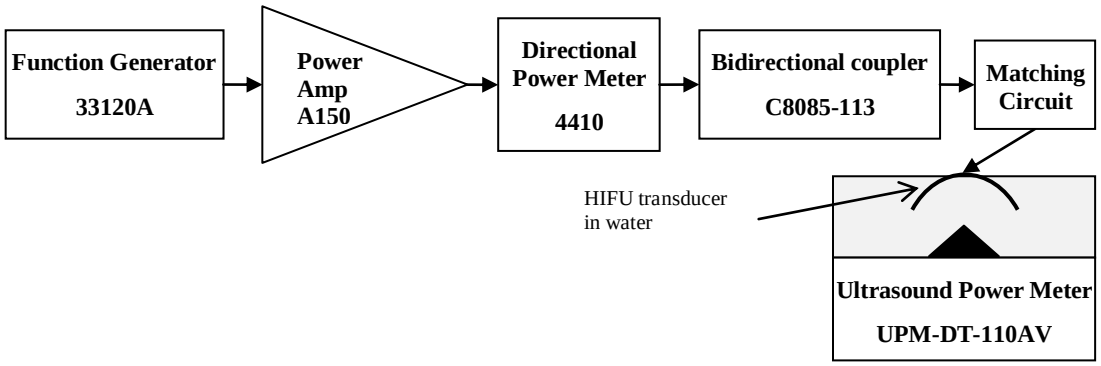

Figure 4 The setup to characterize the electrical and acoustic power efficiency and stability of the HIFU transducer

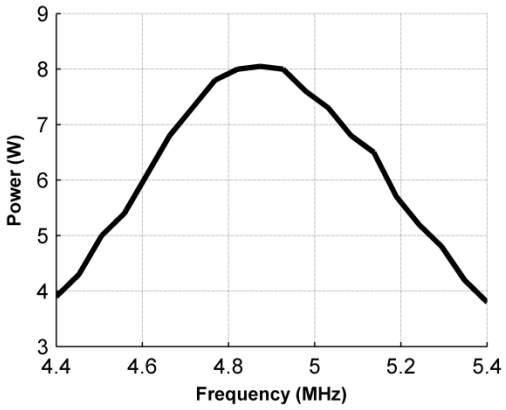

Figure 5 Frequency response measured using an acoustic power meter

Using the same setup, an average acoustic power (p_{ac}) of 23.8W was measured when 33W forward (p_f) electrical power was applied, and a reflected (p_r) electrical power of 1W was measured. The small value for the reflected power indicates satisfactory performance of the electrical matching circuit. The efficiency of the HIFU transducer is calculated as $p_{ac}/(p_f - p_r)$, which equals 74% for this case. The ratio between reflected to forward powers was confirmed using a bidirectional coupler (Werlatone C8085-113).

The long-term transient response of the ultrasound power is shown in Figure 6 (left). The measurement indicates sufficient long-term stability with less than 2.5% power decay over an exposure time of 5 seconds. To evaluate the transducer's repeatability, the acoustic power of five consecutive runs was recorded. Figure 6 (right) shows the power measured at the fifth second of each run. A very small variation is observed. The ratio between the standard deviation of the measurements to its mean is 0.7%. The power meter has a very limited resolution (0.2 W), which poses the main source of error. Enough time delay was given between the runs to insure that HIFU transducer cools down.

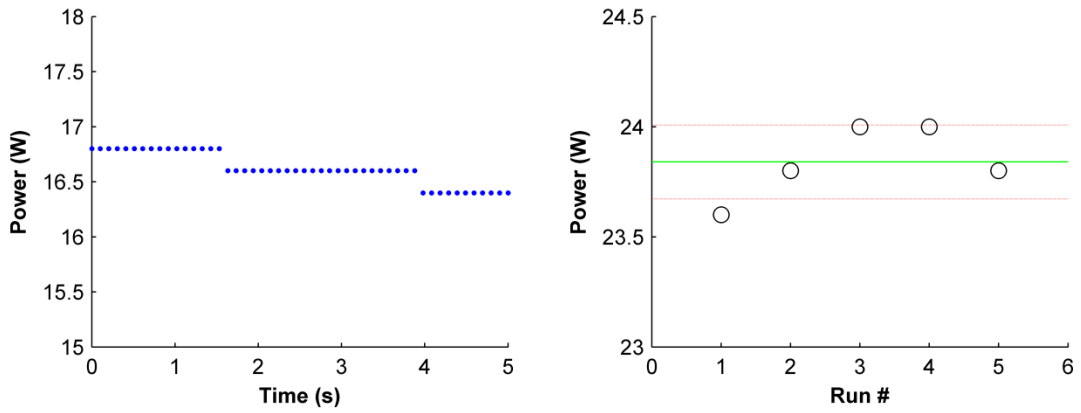

Figure 6 Acoustic power stability over five seconds of continuous stimulation (left), and the power repeatability measured at the fifth second of five runs (right). Means (green) and standard deviation (dotted red) lines are shown

3.2 Mechanically-enhanced hyperthermia

Tissue-mimicking phantoms were used to quantify the proposed *therapeutic gain*. It was shown that gelatin phantoms hardened with glutarldehyde [Nightingale 2001] have stiffness value close to very soft tissues, like liver or breast. As described in Section 2.3, the mechanical resonance of thin constructs of these phantoms was measured in the range of several hundred Hz [Liu 2008]. To make 30 ml of the phantoms solution, 22 ml of water is warmed to 50 ºC, and a specific amount of gelatin is gradually dissolved. A hard phantom (Young's modulus = 1.6 kPa) was made by adding 2 g of gelatin, whereas 1.7 g were added to make phantoms with medium stiffness (Young's modulus = 0.5 kPa). Fabrication of soft phantoms was described [Nightingale 2001] but not used here due to their extreme softness. As scattering particles, 1.9 g of fine graphite spheres are gradually mixed with the solution. Eighteen milliliters of 1-propyl alcohol are added to the mix to adjust the speed of sound and match that in tissue. Before the solution is hardened with 6 ml of glutaraldehyde, the mix is placed in a vacuumed chamber to ensure

degassing. A few minutes in vacuum were found sufficient for degassing and convenient to keep the solution warm enough to harden. The constituents of the phantoms used are given in Table 1.

Table 1 Contents of the tissue-mimicking gels

Content	Medium	Hard
Water (ml)	22	22
Gelatin (g)	2	1.7
Glut. (ml)	6	6
1-Propyl alcohol (ml)	18	18
Fine graphite (g)	1.9	1.9

A very thin thermocouple needle (200 μm) is inserted into the phantoms around 1mm under the surface to record temperature changes. Abrupt index of refraction changes (at the interface of the phantom with the metallic needle) should be avoided to reduce the influence of shock-waves generation. Therefore, the needle was laterally shifted out of the HIFU focus [Hynynen, 1983]. This was achieved by mounting the HIFU transducer on a three-dimensional translational stage. The transducer was stimulated and the temperature measured by the thermocouple was recorded. After finding the position where maximum heat was measured, the transducer was laterally shifted around 0.5 mm. The full-width half-maximum focus of this transducer is close to 1 mm. Data was acquired using a HP's 34901A multiplexer and 34970A DAQ switch unit.

Because of the tissue's immunity to respond to fast stimulus, HIFU modulation was achieved by rectangular modulation. Also, this modulation scheme was chosen because of the simplicity of the circuit generating rectangular pulsing compared to sinusoidal modulation in case this approach was to be incorporated in cwHIFU. Exposures of 5 seconds durations of pHIFU with duty cycles (DC) between 40% and 85%, and pulse repetition frequencies (PRF) in the range of few hundred Hz were applied to the phantoms. The stimulation amplitude was changed for

different duty cycles to ensure conservation of energy, $V_{DC} = V\sqrt{100/DC}$, where V_{DC} is the voltage amplitude at a given duty cycle (DC), and V is the amplitude at full duty cycle. For example, 0.8 V were applied to the RF amplifier at DC = 40%, whereas the applied voltage was equal to 0.55 V at 85% DC. The transducer described in the previous subsection was used as a HIFU applicator. Stimulation was generated by a Spartan 3 FPGA and amplified by an RF power amplifier. The data acquisition system (DAQ 3497 A) was connected to a PC acquiring the recorded temperate data. The setup is shown in Figure 7.

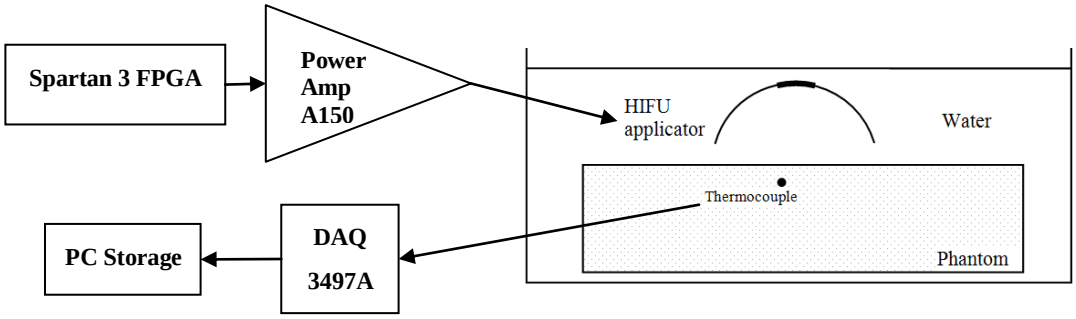

Figure 7 The pHIFU experiment setup. The figure shows the phantom immersed in water, the HIFU applicator (the dark segment is the imaging transducer segment), and the thermocouple

Chapter 4: Experimental results

With different pulsing parameters, temperature in proximity of the HIFU focus was continuously recorded for 15 seconds. One second was recorded before the onset of pHIFU, and the last 9 s were recorded after the stimulation is terminated. Figure 8 shows the exponential temperature changes in a 10mm thick phantom with young's modulus of 1.6 kPa. Displayed curve share the same DC of 85% and a PRF varying between 200 and 800 Hz, where darker lines correspond to lower PRF. Because of hardware limitations, the generation of full duty cycles was not possible. The absence of transient changes at the PRF in the curves means that modulation frequency of the stimulation is faster than the thermal transient response. Roughly, higher temperature rise is observed at higher PRF.

The same test was run using other duty cycles (40%, 55% and 70%), temperature measurements at different time points (0.1, 0.6, 1.2, 1.8, 2.4, 3.0, 3.6, 4.2 and 4.8 seconds after the onset of pHIFU) are shown in Figure 9 as a function of DC. It is clear that higher temperatures are measured at higher DC. The similarity in the trends at different time instances indicates the systematic response of the measurement.

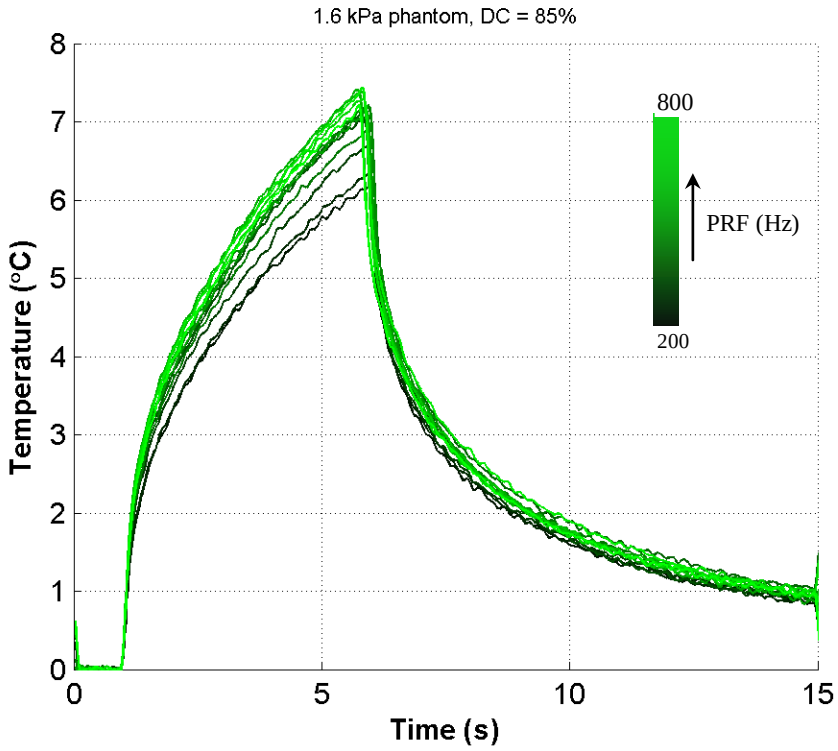

Figure 8 Temperature measured at 85% duty cycle and PRF varying between 200 and 800 Hz with a step of 50 Hz

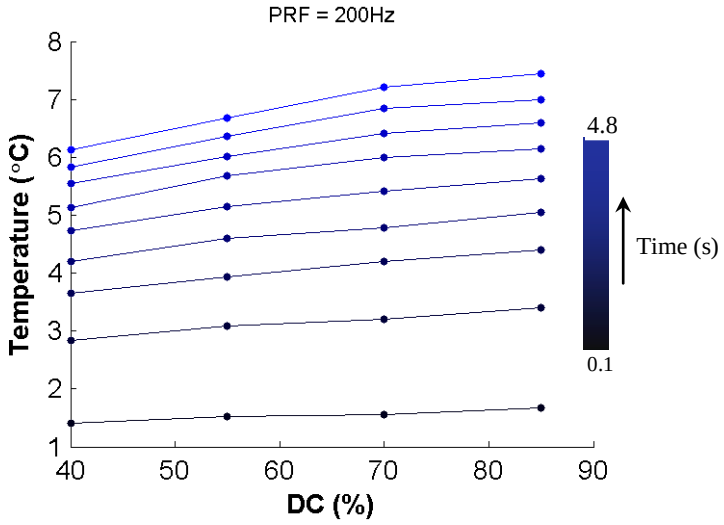

Figure 9 Temperature measured at different time points after pHIFU onset versus duty cycle

To understand the influence of PRF on temperature changes, normalized temperature maps as a function of time and PRF are shown in Figure 10 for DC=40% (a) and DC=85% (b). Maps collected with 40% duty cycle (Figure 10(a)) are showing obvious dependence of heat generation on PRF. For the tested phantom, heat generation peaks at PRF = 800 Hz. Local maxima were also observed at 500 and 650 Hz. Similar relation for data acquired at higher duty cycle, 85%, is displayed in Figure 10(b) showing decreased specificity of heat enhancement as a function of PRF, suggesting a role of duty cycle in the optimization process.

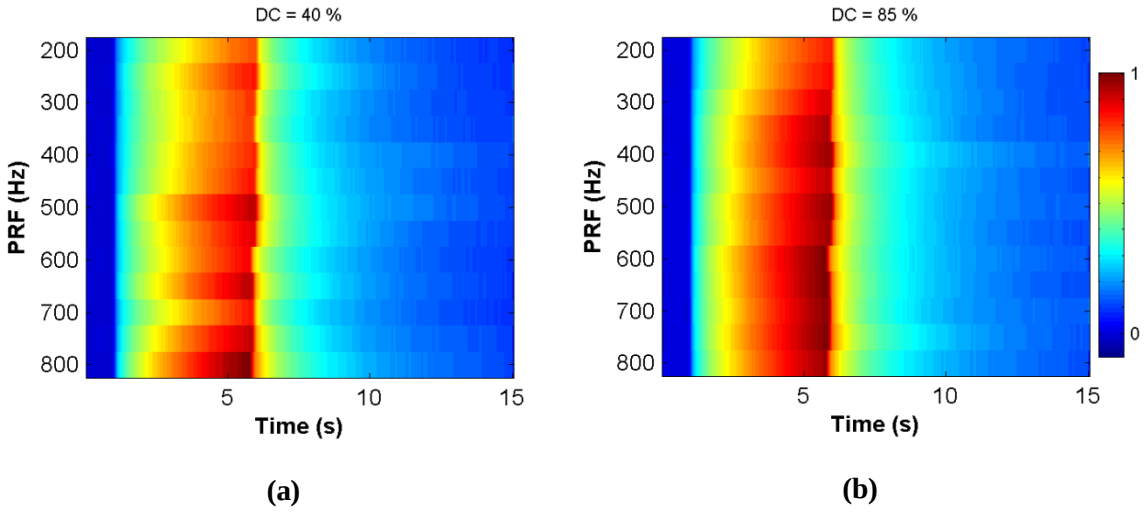

Figure 10 Normalized temperature as a function of PRF and time shown at fixed duty cycle (a) 40% and (b) 85%

Figure 11 shows the measured temperature as a function of duty cycle and time, measured at 200 and 750 pulse repetition frequencies. The plots show that temperature enhancement is proportional to pulsing duty cycle. Higher temperatures are measured at higher duty cycles, i.e. lower modulation voltage.

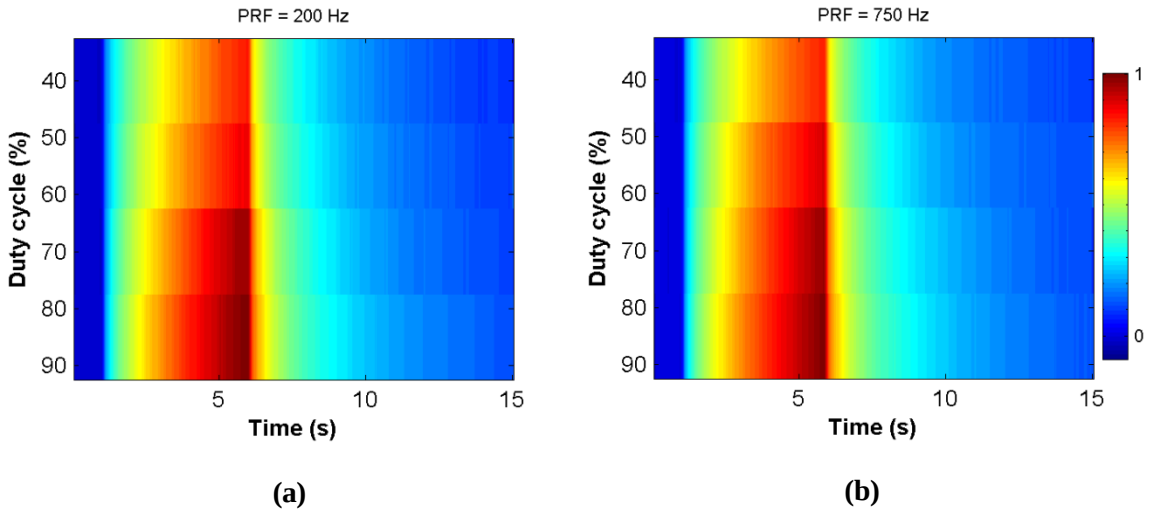

Figure 11 Normalized temperature as a function of duty cycle and time shown at fixed PRF (a) 200 Hz and (b) 750 Hz

Plots in Figure 12 show normalized temperature maps versus PRF and DC at different time instances after pHIFU onset. Each plot is individually normalized. The plots show that, despite the conservation of electrical energy, improved thermal generation is achieved at specific PRF-DC combinations. The plots show that enhancement is a time invariant function, suggesting a consistency of the enhancement regardless of the length of the exposure. For each of the nine plots in Figure 12 (i.e. different time instances t), the enhancement factor ε_t is defined as:

$$\varepsilon_t = \frac{\Delta T}{T_{min}}\bigg|_t \times 100\% \tag{6}$$

where ΔT is the difference (maximum minus minimum) in the temperature at a given time instance, and $T_{\min}$ is the minimum temperature observes at the same time instance. Using Equation 6, enhancement factors are calculated at each time instance. For each time instance shown in Figure 12, the mean enhancement factor is 48% with a standard deviation of 2.5%. This indicates a considerable enhancement achieved by pulsing HIFU at the mechanical resonance of

the phantom. The right-most vertical line in these plots would have presumably been constant if full duty cycles were achievable.

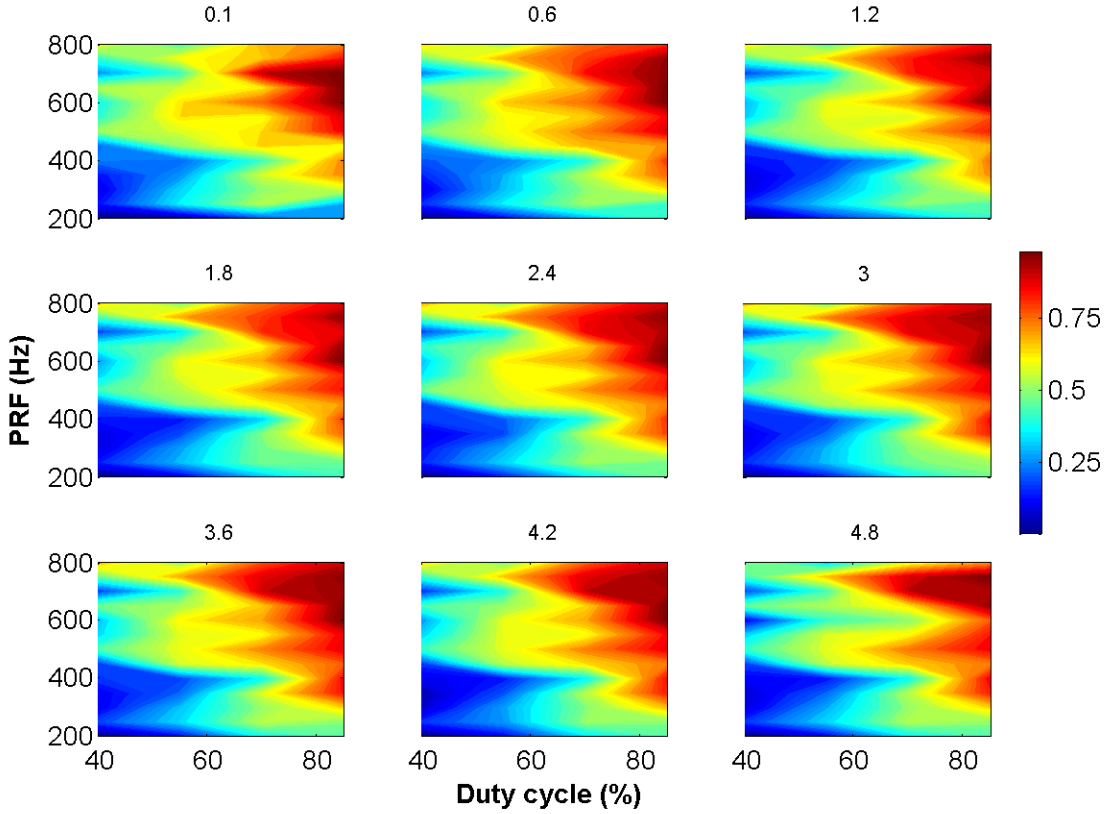

Figure 12 Normalized temperature measured at different times versus PRF and DC. Time elapsed after pHIFU onset is shown on top of each plot. Data was collected for thick (10 mm) hard (1.6 kPa) phantom

Figure 13 and Figure 14 show similar plots for a thin (3.8mm) hard phantom, and a thick medium (0.5kPa) phantom, respectively. Similar trends of heat enhancement are exhibited by the three tested phantoms, with mean and standard deviation enhancement factors of 37% and 3.6% for the thin hard phantom, and 41% and 3.3% for thick medium phantom, respectively. Nevertheless, the plots show that enhancement is not shapely peaked, and could be observed at different PRF–DC combinations. This effect may be attributed to the mechanical properties of the phantoms, and to the rectangular wave modulation resulting in odd harmonic generation of the

modulation frequencies. This means that in a phantom exhibiting resonance at 150 Hz, for example, and due to significant harmonics of the rectangular signal modulation, there will be local maxima observed at 450, and 750 Hz too.

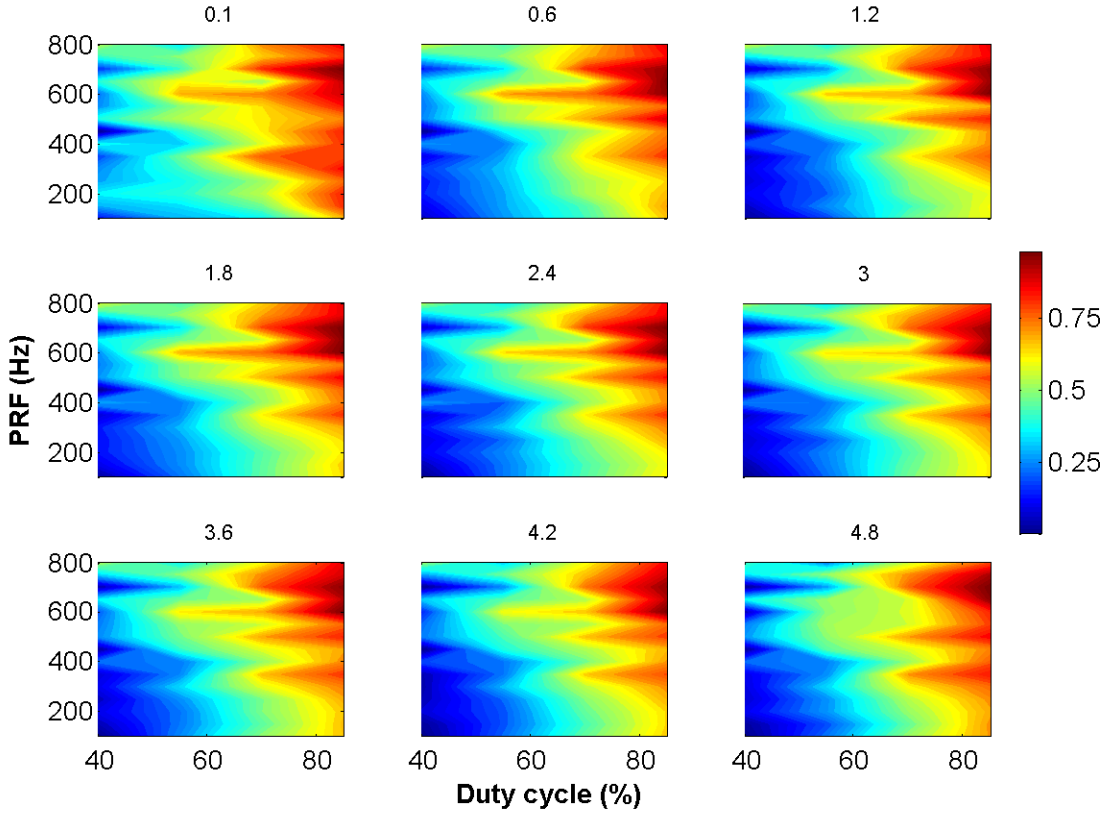

Figure 13 Normalized temperature plots for thin (3.8 mm) hard (1.6 kPa) phantom

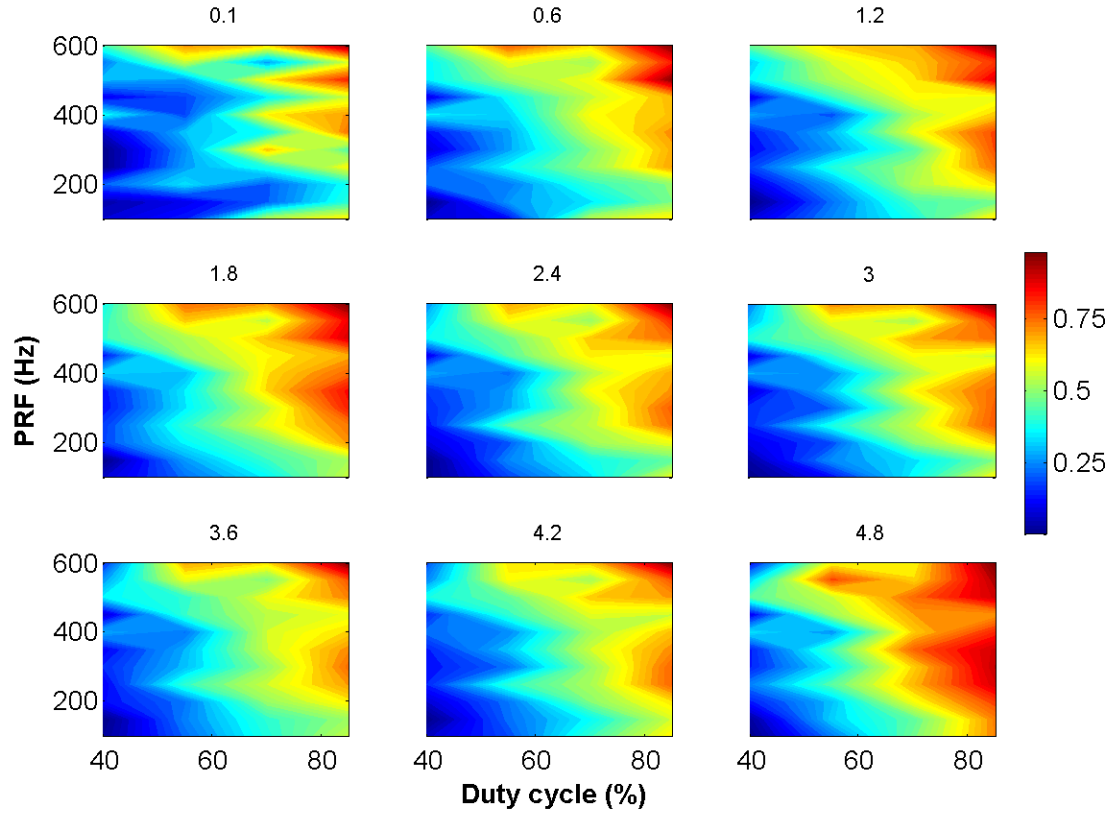

Figure 14 Normalized temperature plots for thick (10 mm) medium (0.5 kPa) phantom

Although the same amount of acoustic energy is deposited into the phantoms, direct proportionality is observed between higher duty cycles of pHIFU stimulation and temperature. As described in Section 2.1, this effect is not explained by the tBHTE. Nonlinear interaction, which is not considered in the tBHTE, may explain this observation.

To evaluate nonlinear wave generation, pulsed stimulation was again applied to the transducer, and the acoustic wave in water medium was measured using a hydrophone (500µm, TNU001A, NTR systems, Inc.). The detected signal was amplified using a 30 dB preamplifier (NTR systems, Inc.). Figure 15, shows the outputs measured at different stimulation amplitudes, corresponding to the different duty cycles. Spectral information is shown underneath each

corresponding recording. At 50 mV, the measured wave is dominated by pure stimulation frequency (3.78 MHz in this case, a different transducer with comparable geometry was used in this experiment). As the amplitude increase, higher harmonics generate due to nonlinearity.

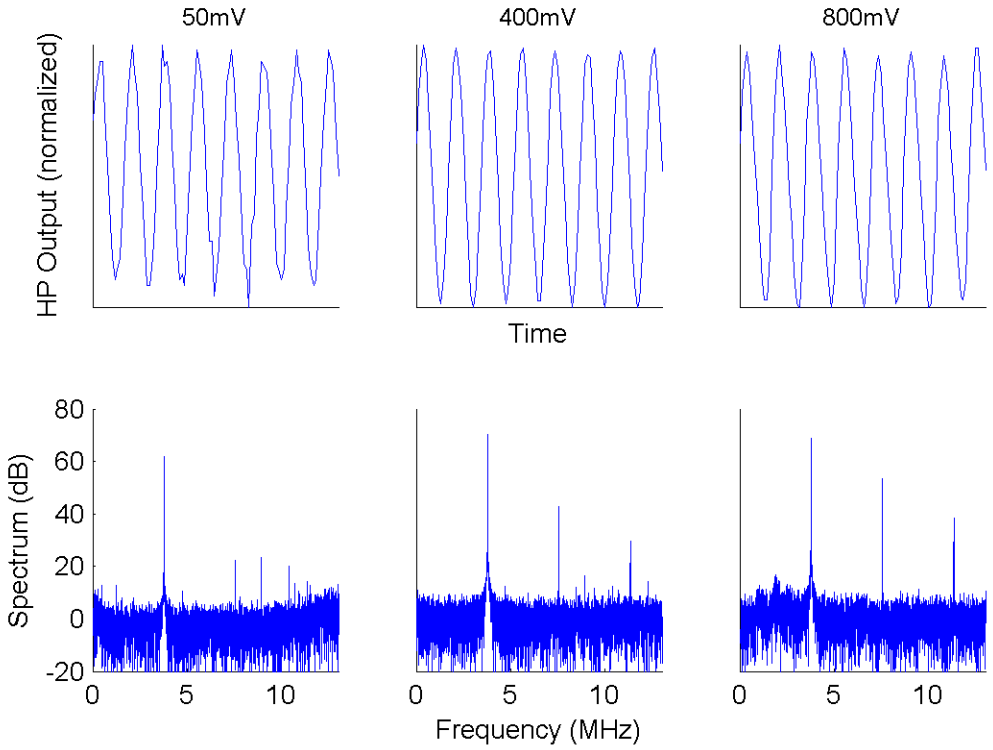

Figure 15 Normalized HIFU signal recorded by the hydrophone at different amplitudes (top), and the corresponding spectra showing increased nonlinearity at higher intensities (bottom)

Figure 16 shows the spectral amplitudes at the harmonics of the measured acoustic signal versus the input voltage. As expected, the difference between the fundamental and higher harmonics decreases as the applied voltage increases. Given the voltage range used in the heating experiments (550 - 800 mV), the experiments have shown more heating at higher duty cycles, that is, relatively low stimulation amplitudes; implying that nonlinearity may have resulted in

prefocal absorption at lower DC. If the experiments were operated at purely linear regime, there must be no DC dependence as discussed in Section 2.1 and demonstrated in the next chapter.

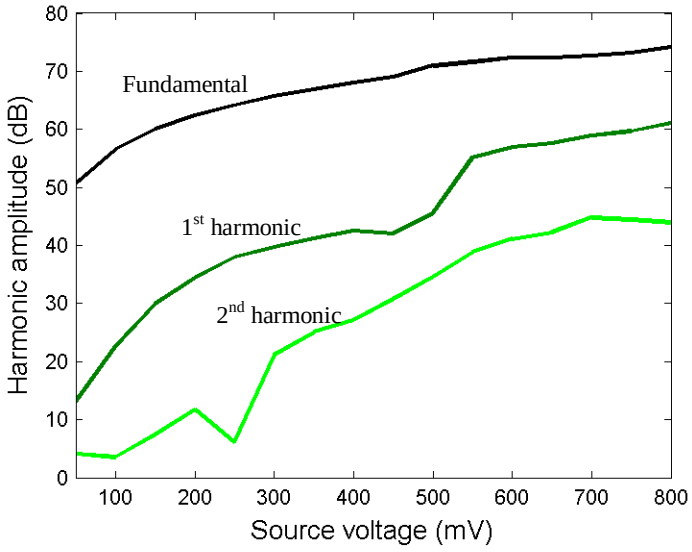

Figure 16 First, second and third harmonics (darker to lighter) at different stimulus intensities

Chapter 5: Equivalent model

In this chapter, a model describing the interaction between HIFU wave and the tissue mimicking phantom is introduced. The model does not account for the mechanical response of the phantoms. Therefore, the influence of PRF on the heating experiments can not be studied. COMSOL software was used to implement a multiphysics finite element model of the phantom. The actual geometry of the transducer used in the experiments was considered.

The speed of sound is calculated as 1492 m/s and 1512 m/s for water and phantoms, respectively [Liu 2008]. The density (ρ_0) of both was used as 1100 (kg/m^3), and the wavenumber was set to 1500 m^{-1}. The initial pressure condition was set to zero Pascal. According to the derivation in [Morse 1987, P. 263], acoustic intensity (I) is found from the calculated acoustic pressure (p) and particle velocity (v) along the two-dimensional spatial coordinates. Temperature was calculated using the Bioheat equation described in Section 2.1, and setting the absorption coefficient (α) to 0.45 [Liu 2008], the thermal conductivity (k) to 0.58 W.m^{-1}.K^{-1}, and the heat capacity to C_p = 4.181 J.g^{-1}.K^{-1} [CRC 2009-2010].

Considering the wavelength, the geometry of the model is large. Performing interpolation in COMSOL allows reducing the maximum element size of the triangular meshes to one fifth of the wavelength without significant frequency dispersion [Taflov 2005]. This has minimized the computational demand of the model.

Figure 17 shows the model geometry and maps of calculated temperature at the onset of HIFU, and after 5 seconds of continuous stimulation. The geometry shows a 2D cross-section section of the setup, the transducer immersed in water, and the phantom with the thermocouple needle inside. HIFU stimulation emanates from the two curves representing the transducer segments. The waves propagate in water then phantom, where the acoustic wave is absorbed into

thermal energy. The boundaries on the bottom and sides of the phantom are set as hard boundaries resulting in reflections of the acoustic waves.

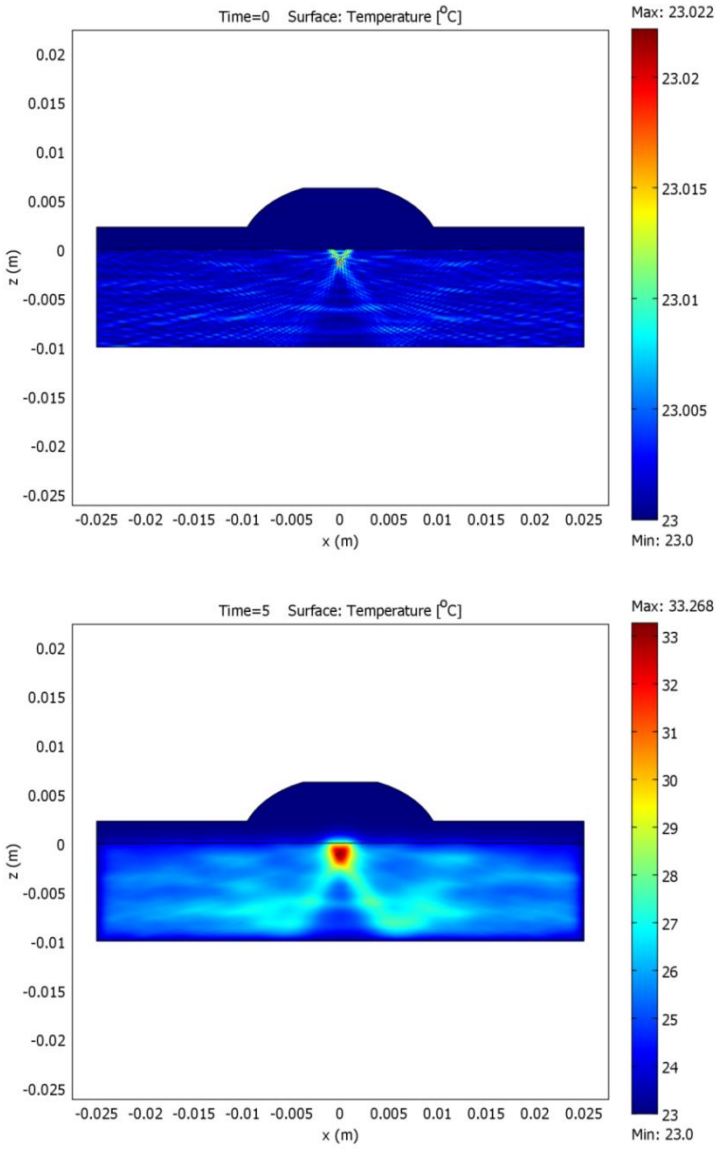

Figure 17 Calculated temperature maps at the instance of HIFU application (top), and at the fifth second after continuous application (bottom)

To prove that in a strictly thermal modal (no mechanical energy is calculated) the generated heat is independent of PRF, HIFU stimulation was pulsed at the same PRF values used in the experiments. A duty cycle of 70% was used for all seven runs. Figure 18 shows the normalized temperature values calculated using pHIFU. This result supports the claim in Section 2.1 that the tBHTE is a narrowband LP filter. It also confirms that the PRF dependence shown in Chapter 4 is not due direct thermal absorption of the acoustic energy.

In these runs, high temporal resolution was required to guarantee reasonable representation of the pulsing waveform. This has significantly increased the computational demand of the model. Therefore, in addition to reducing the analysis time, the entire geometry was reduced to 20 mm laterally and 6 mm axially measured from the phantom interface with water. To reduce the effect of acoustic reflections from the close boundaries in this geometry, the boundary conditions at the phantom container (bottom and sides) were changed to soft boundaries, i.e. the mismatch between the indices of refraction at the interface was reduced.

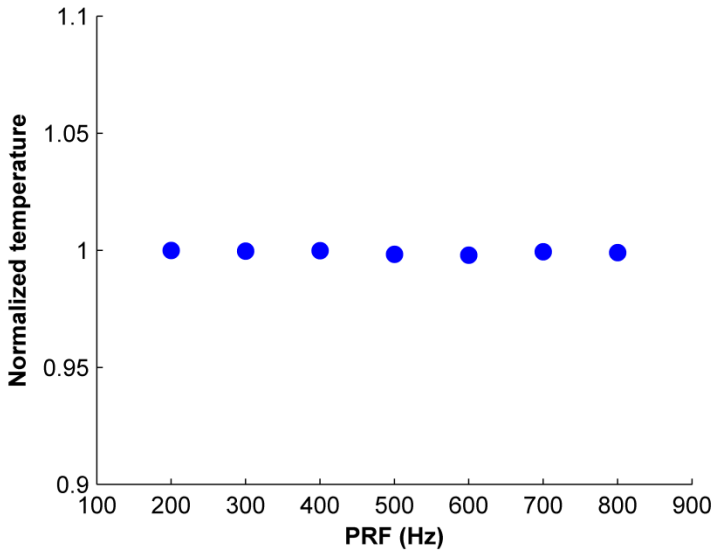

Figure 18 Normalized temperature calculated at different PRF

To investigate the influence DC on the generated heat, pHIFU stimulation was pulsed at different duty cycles at a fixed PRF of 100 Hz. The same geometry used to the last experiment (variable PRF, fixed DC) was also used. Normalized temperature curves for 40%, 70% and a full duty cycle are shown in Figure 19. Contrary to the experimental results shown in Chapter 4, the model suggests that heat generation is independent from the duty cycle. The discrepancy is attributed to the linear response of the model, which does not account nonlinear interaction. Higher harmonics generated at lower duty cycles (higher stimulation voltage) have a higher absorption coefficient. Hence, they may be prefocally absorbed, limiting the acoustic intensity reaching to focus. Even if harmonics are generated but not prefocally absorbed, the tighter focus of the higher harmonics may have less impact on the signal measured by the thermocouple placed outside the focus.

The modulations observed on the 40% and 70% DC plots in Figure 19 were less pronounced in the experimental work shown in Figure 8. This is maybe due to the low-pass response of the RF amplifier and the HIFU applicator which smoothes out the rectangular modulation created at the FPGA. The frequency response of the thermocouple needle may also have a significant contribution in this smoothing effect.

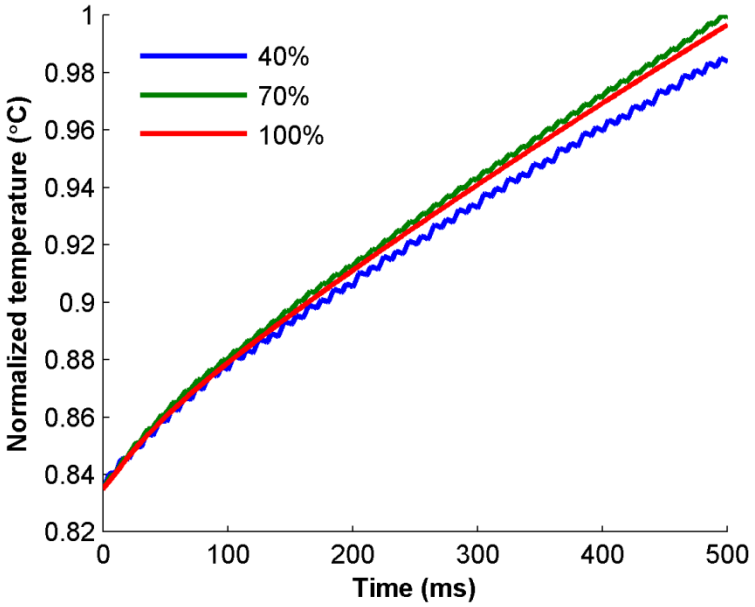

Figure 19 Normalized temperature rise calculated with different duty cycles of pHIFU modulation

Although harmonics generation can not be investigated using this model, the influence of diffraction on harmonics can be visualized by stimulating the transducer at a harmonic frequency. HIFU beam shape was calculated under the influence of fundamental stimulation frequency (5 MHz), and the calculation was repeated using 10 MHz stimulation (equivalent to second harmonic). Figure 20 shows the calculated temperature at different time instances in proximity of the thermal focus. The figures show tighter focus under the second harmonic stimulation; which may contribute in an apparent DC dependence of the *therapeutic gain* (due to larger separation between the thermocouple and the focus), and the absence of PRF modulation on the experimental temperature evolution curves (Figure 8).

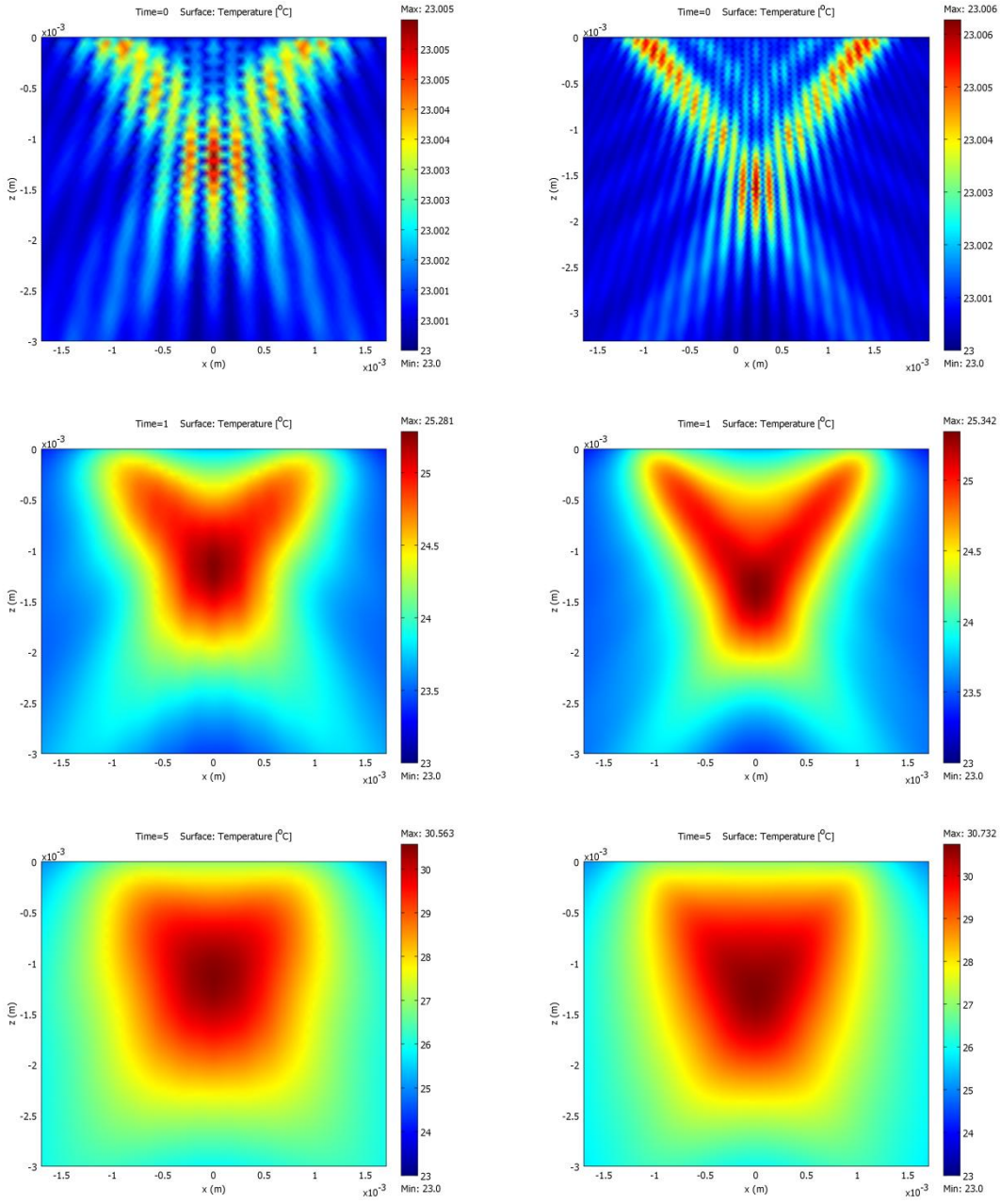

Figure 20 Temperature maps calculated at different time instances in proximity of thermal focus point. The left column shows results from 5 MHz cwHIFU stimulation, while the right column shows outputs calculated from 10 MHz cwHIFU stimulation

Chapter 6: Discussion

The *therapeutic gain* of HIFU operation in pulsed mode was evaluated. Temperature rise due to pHIFU application was measured using a thermocouple needle inserted in tissue mimicking phantoms. Experiments with different PRF and DC were executed considering conservation of electrical energy. One can find that most of pHIFU studies in literature are not clearly introducing the basis of choosing pulsing frequency and its duty cycle. Pulsing parameters in this study, however, were exploited to achieve precious *therapeutic gain*. We conclude that pulsing HIFU at the mechanical resonance of the phantoms helps transforming the mechanical energy into a thermal form.

Modulation parameters of pHIFU were found significant in optimizing the therapeutic window. The enhancement is dependent on the PRF of the modulating rectangular wave. Description in Section 2.1 and the outcome of the numerical model in Chapter 5 show that in a strictly thermal model, heating should be independent from PRF at the frequency range used. PRF dependence is attributed to the mechanical properties of the phantoms. When pHIFU is pulsed at the mechanical resonance of the medium, shears waves are continuously generated and eventually absorbed as thermal energy. This mode of energy conversion leads to higher concentration of heating near the focal spot.

Enhancement was found also proportional to pulsing duty cycle. This could possibly be described by prefocal energy loss due to nonlinearity. Higher harmonics of the propagating acoustic wave will generate even at low acoustic intensities, this phenomenon is known as finite-amplitude distortion. Because the acoustic pressure oscillates with the applied intensity, the local density of the medium, and therefore the local speed of sound will be altered as the pressure changes. The different speeds of the wave distort the sinusoidal wave, more as the pressure increases, generating higher harmonics as the wave propagates [Hamilton 1997, P. 107]. As

described in Section 2.4, higher harmonics get absorbed faster. Therefore, if harmonics were generated prefocally, acoustic energy maybe absorbed before reaching the focal point reducing energy deposited at focus. Prefocal absorption may be avoided by keeping the stimulation intensity of HIFU applicator lower than intensity saturation (a point when severe nonlinearity is generated). This procedure, however, is far from trivial. The acoustic frequency, applicator geometry, and the propagating medium must be taken into account.

Based on the hydrophone's measurements, some level of nonlinearity was observed. Since electrical energy conservation is observed, stimulation voltage is higher at lower duty cycles. Therefore, nonlinear interaction is higher at lower DC, and increased prefocal absorption may reduce the energy deposited at the focus nearby the thermocouple. This assumption is supported by the description in Section 2.1, and the results of the numerical model: in a linear regime, pulsing HIFU at the parameters used in this study does not influence the direct heat deposition ($2\alpha I$) if energy conservation is observed.

Another possible explanation of the observed DC dependence can be the diffraction effect, which is another nonlinear effect described in Section 2.4 and shown in Figure 20. Tighter foci correspond to higher harmonics; which means that in case when the second harmonic, for example, was generated nearby the focus and was not prefocally absorbed, its heating focus will be farther from the thermocouple needle, and the sensed temperature will not represent the actual temperature in focus. This assumption, however, was tested in the model by measuring the temperature at the actual thermocouple location for both 5 and 10 MHz stimulations, and no significant difference was observed.

Two-dimensional thermal imaging or inclusive modeling is required to evaluate the nonlinearity influence on the measurements. Non-invasive temperature estimation techniques are

possible using ultrasound imaging [Simon 1998, Liu 2010], or optical coherence tomography [Adler 2004]. Uncertainties in the measurements can arise from inaccurate placement of the thermocouple needle. Although precise alignment was done as described in Section 3.2, measurement of the axial and/or lateral temperature profile would have helped. Imaging the exact location of the needle could have yielded higher certainty.

Controlled optimization is better achieved under linear absorption of the acoustic wave in the tissue. Nonlinear effect, however, can be exploited to potentially play a role in enhancing the therapeutic window. Since wave-tissue interaction is dependent on the medium and its boundaries, determining the resonance of the target tissue will be easier using an experimental method as the one described in [Liu 2008]. A pre-surgical interrogation of the target tissue is an easy method to maximize the therapeutic outcome.

This work has shown that pHIFU can introduce potentially valuable *therapeutic gain*. The optimization parameters are shown to vary with the mechanical properties of the tissue, and its boundaries. The results show a 50% *therapeutic gain* by pulsing HIFU at the mechanical resonance of the tissue, and with high duty cycles. Benefiting from the high attenuation of the mechanical shear waves, the achieved *therapeutic gain* is possibly more localized.

Bibliography

Adler D, Huang S, Huber R, and Fujimoto J, (2008). Photothermal detection of gold nanoparticles using phase-sensitive optical coherence tomography. *Optics Express*, **16**, 4376-4393

Arefiev A, Prat F, Chapelon J, Tavakkoli J, and Cathignol D, (1998). Ultrasoundinduced tissue ablation: Studies on isolated, perfused porcine liver. *Ultrasound in Medicine and Biology*, **24**, 1033–1043

Child S, Vives B, Fridd C, Hare J, Linke C, Davis H, and Cerstensen E, (1980). Ultrasonic treatment of tumors – II, moderate hyperthermia. *Ultrasound in Medicine and Biology* , **6**, 341 - 344

Cobbold R, (2006). Foundations of biomedical ultrasound, *Oxford University press, USA*

Dittmer K, Jianwu X, Finie H, Cameron T, Monica B, Victor F, and King C, (2005). Pulsed High-Intensity Focused Ultrasound Enhances Systemic Administration of Naked DNA in Squamous Cell Carcinoma Model: Initial Experience. *Radiology* , **235**, 541 - 546

Douglas M, (2000). Empirical relationships between acoustic parameters in human soft tissues. *Acoustics Research Letters Online*, **1** (2), 37-42

Dromi S, Frenkel V, Luk A, Traughbe B, Angstadt M, Bur M, Poff J, Xie J, Libutti S, Li K, and Wood B, (2007). Pulsed-High Intensity Focused Ultrasound and Low Temperature-Sensitive Liposomes for EnhancedTargeted Drug Delivery and Antitumor Effect. *Clinical Cancer Research* , **13** (9), 2722 – 2727

Ebbini E, (1990). Deep localized hyperthermia with ultrasound phased arrays using the pseudoinverse pattern synthesis method. Ph.D. dissertation, University of Illinois.

Frenkel V, and Li K, (2006). Potential role of pulsed-high intensity focused ultrasound in gene therapy. *Future Oncology* , **2** (1), 111 - 119

Foster F S, Lockwood G R, Ryan L K, Harasiewicz K A, Berube L, and Rauth A M, (1993). Principles and applications of ultrasound backscatter microscopy. *IEEE Transactions on Ultrasonics, Ferroelectrics and Frequency Control*. **40**(5), 608-617

Goss S A, Frizzell L A, and Dunn F (01979). Dependence of the ultrasonic properties of biological tissue on constituent proteins. *Journal of the Acoustical Society of America*. **67**(3), 1041-1044

Goss S A, and Fry F J, (1981). Nonlinear Acoustic Behavior in Focused Ultrasonic Fields- Observations of Intensity Dependent Absorption in Biological Tissue. *IEEE Transactions on Sonics and Ultrasonics*. **28(**1), 21 - 25

Hamilton F, and Blackstock D, (1997). Nonlinear Acoustics: Theory and Applications. First edition. *Academic press*

CRC (2009-2010). Handbook of Chemistry and Physics. Boca Raton, 90th edition, 6-1.

Hynynen, K. (1985). Nonlinear absorption during scanned focused ultrasound hyperthermia. *Ultrasonics Symposium* , 925 - 929.

Hynynen K, Martin C, Watmough D, and Mallard J, (1983). Errors in temperature measurement by thermocouple probes during ultrasound induced hyperthermia. *The British Journal of Radiology* , **56**, 969 - 970.

Kennedy J, Ter Haar G, and Cranston D, (2003). High intensity focused ultrasound: surgery of the future? *The British Journal of Radiology* , **76**, 590–599.

Morse P, and Ingard K, (1987). Theoretical Acoustics. *Princeton University Press*

Lee C, and Wang T, (1993). Acoustic radiation pressure. *Journal of Acoustic Society of America*, **94** (2) 1099-1109

Liu D, and Ebbini E, (2008). Viscoelastic propery measurement in thin tissue constructs using ultrasound, *IEEE Transactions on Ultrasonics, Ferroelectrics, and Frquency Control*, **55** (2), 368 – 383

Liu D, and Ebbini E, (2010). Real-Time 2-D Temperature Imaging Using Ultrasound. *IEEE Transactions on Biomedical Engineering*, **57** (1), 12-16

Morgan Electroceramics, Piezoelectric Ceramics Properties & Applications

Morse P, and Ingard K, (1987). Thoeritical acoustics. Princeton University Press

Muir T G, and Carstensen E L, (1980). Prediction of nonlinear acoustic effects at biomedical frequencies and intensities. *Ultrasound Medicine and Biology* , **6** (4), 345 - 357

Nassiri D K, and Hill C R, (1986).The differential and total bulk acoustic scattering cross sections of some human and animal tissues. *Journal of the Acoustical Society of America*, **79** (6), 2034-2047

Nightingale K, Palmeri M, Nightingale R, and and Trahey G, (2001). On the feasibility of remote palpation using acoustic radiation force. *Journal of the Acoustical Society of America* , **110** (1), 625 - 634

Ninet J, Roques X, Seitelberger R, Deville C, Pomar J L, Robin J, Jegaden O, Wellens F, Wolner E, Vedrinne C, Gottardi R, Orrit J, Billes M, Hoffmann D, Cox J L, and Champsaur G, (2005). Surgical ablation of atrial fibrillation with off-pump, epicardial, high-intensity focused ultrasound: Results of a multicenter trial. *The journal of thoracic and cardiovascular surgery*, **130** (3), 803.e1-803.e8

Pennes H, (1948).Analysis of tissue and arterial blood temperature in the resting human forearm. Jourdnal of Applied Physiology, **1** (2), 93-122

Sapareto S, and Dewey W, (1984). Thermal dose determination in cancer therapy. *International Journal of Radiation Oncology Biology Physics*, **10**, 787-800.

Sarvazyan A, Rudenko O, Swanson S, Fowlkes B, and Emelianov S, (1998). Shear wave elasticity imaging: a new ultrasound technology of medical diagnostics. *Ultrasound in Medicine and Biology* , **n4** (9), 1419 - 1435

Schmidt B, Chun J, Kuck K, and Antz M, (2006). Pulmonary vein isolation by high intensity focused ultrasound. *Indian pacing and electrophysiology journal* , **7** (2), 126 - 133.

Simon C, VanBaren P, and Ebbini ES, (1998). Two-dimensional temperature estimation using diagnostic ultrasound. *IEEE Transactions on Ultrasonics, Ferroelectrics and Frequency Control*, **45**, 1088-1099

Swindell W, (1985). A theoretical study of nonlinear effects with focused ultrasound in tissues: an acoustic bragg peak. *Ultrasound in Medicine and Biology* , **11** (1), 121 - 130

Taflove A, and Hagness S. C., (2005). Computational Electrodynamics: The Finite-Difference Time-Domain Method. Artech House Publishers

Tachibana K, and Tachibana S, (2001). The Use of Ultrasound for Drug Delivery. *Echocardiography*, **18**(4), 323-328

Thomas C R, Farny C H, Coussios C C, Roy R A, and Holt R G, (2005). Dynamics and control of cavitation during high intensity focused ultrasound application. *Acoustics Research Letters Online.* , **6**, 182 – 187

Tobis J M, Mallery J, Mahon Do, Lehmann K, Zalesky Pa, Griffith J, Gessert J, Moriuchi M, McRae M, Dwyer M-L, Greep N, and Henry W L, (1991). Intravascular Ultrasound Imaging of Human Coronary Arteries in Vivo Analysis of Tissue Characterizations With Comparison to In Vitro Histological Specimens. *Circulation, American Heart Association*, **83**, 913-926

Wu F, Wang Z, Cao Y, Chen W, Bai J, Zou J, and Zhu H, (2003). A randomised clinical trial of high-intensity focused ultrasound ablation for the treatment of patients with localised breast cancer. *British Journal of Cancer*, **89**, 2227 – 2233